Applied Water Science (2025) 15:200
https://doi.org/10.1007/s13201-025-02566-3

ORIGINAL ARTICLE

In silico design and simulation of graphene oxide-based metal–organic framework nanomaterial for water purification

Mahnaz Shahabi[1,2] · **Ali Ahmadpour**[1,2] · **Heidar Raissi**[3]

Received: 26 January 2025 / Accepted: 17 June 2025

Abstract

The widespread presence of microplastics (MPs) in water has become an environmental concern due to their adverse effects on human health and aquatic ecosystems. To address this issue, metal–organic framework/graphene oxide composites have recently emerged as a promising solution for wastewater treatment due to their unique properties such as high loading capacity and enhanced stability. In this research, the uptake mechanisms of two types of MPs, including Polyamide 66 (PA66) and Polyurethane (PU) based on the metal–organic framework Cu-BTC/graphene oxide (Cu-BTC/GO) composite, are evaluated by molecular dynamics (MD) simulation. By increasing the number of adsorption sites through the incorporation of GO onto Cu-BTC, the designed composite demonstrates higher efficiency in removing MPs compared to the pristine MOF. The removal percentage of PA66 and PU increases from 25% and 0.75% in the MP-single Cu-BTC systems to 100% upon adsorption in the Cu-BTC/GO composite, respectively. The adsorption capacity of Cu-BTC/GO composite for MPs is enhanced through π–π stacking, C–H$\cdots$ π interactions, hydrogen-bonding network, and electrostatic attractions, with a predominant hydrophobic nature. Furthermore, the results of density functional theory (DFT) calculations confirm the findings from the MD study. This research provides detailed atomistic insights into the mechanisms of microplastics removal by the metal–organic framework composite with graphene oxide from wastewater.

Keywords Microplastic · Water treatment · Polyamide 66 · Polyurethane · Cu-BTC/GO composite · Molecular dynamics simulation

Introduction

In recent years, the development of industrial and human activities has led the release of textile industries and organic compounds into the air, water, and soil. Nowadays, microplastics (MPs) are an emerging threat to wildlife and human health due to their inherently persistent and non-biodegradable nature (Cole et al. 2011). They can be detected in the food chain and webs as well as in personal and baby care products and cause many adverse effects on human and animal health (Kang et al. 2019). Hence, the removal of MPs becomes an intractable environmental concern in aquatic ecosystems.

The strategies for removing pollution in the environment are mainly photocatalysis (Karami et al. 2022; Guo et al. 2020; Tabatabaeinejad et al. 2021; Yousefzadeh et al. 2023), electrochemistry (Chen et al. 2004; Mu et al. 2009), biodegradation (Zhou et al. 2021; Varjani et al. 2020; Hosseini et al. 2024), membrane filtration (Wu et al. 1998; Neghlani et al. 2011), and adsorption (Azadpour et al. 2021; Othmani et al. 2021; Pourmand et al. 2025; Ali et al. 2012). Among these methods, the adsorption technique has attracted a considerable attention due to its simplicity, high efficiency, compatibility with the environment and low cost (Ali et al. 2012; Liu et al. 2019).

✉ Ali Ahmadpour
ahmadpour@um.ac.ir

Mahnaz Shahabi
m.shahabi@um.ac.ir

Heidar Raissi
hraeisi@birjand.ac.ir

[1] Department of Chemical Engineering, Faculty of Engineering, Ferdowsi University of Mashhad, Mashhad, Iran

[2] Industrial Catalysts and Adsorbents and Environment Laboratory, Oil and Gas Research Institute, Ferdowsi University of Mashhad, Mashhad, Iran

[3] Department of Chemistry, University of Birjand, Birjand, Iran

Published online: 10 July 2025

Metal–organic frameworks (MOFs) are highly attractive porous materials for the adsorption removal of pollutants (Wan et al. 2022; Chen et al. 2020) and other industrial applications (Stock et al. 2012) due to their large specific surface area, pore volume (Millward et al. 2005), tunable pore morphology, and rich surface chemistry (Botas et al. 2011; Mulfort et al. 2007). However, the low stability of MOFs in humid conditions poses a significant challenge to their practical applications (DeCoste et al. 2013). To address this issue, incorporating other microporous (Górka et al. 2010; O'Neill et al. 2010) or layered materials (Petit and Bandosz 2011; Xiang et al. 2011) into their structures can alter their physicochemical properties. Carbon-based nanostructures are identified as suitable complementary materials for the synthesis of MOF composites due to their low toxicity, mechanical strength, and chemical resistance (Hamzeh Ali et al. 2020; Varghese et al. 2021). Graphene oxide (GO), characterized by its large surface area, oxygen-containing functional groups, and inherent hydrophobicity, is an emerging material for MOF composites (Petit and Bandosz 2009). The combination of GO with MOFs enhances porosity and dispersion forces, as well as improving material stability and adsorption performance (Levasseur et al. 2010). Research has shown that loading GO onto the MOF surface significantly increases water stability (Dahanayaka et al. 2020; Bhoria et al. 2020; Domán et al. 2020; Sui et al. 2019). As proven by many experimental and theoretical researches, MOF/graphene-based material composites are effective in removing various pollutants (Wan et al. 2022; Petit et al. 2010; Zhao et al. 2013; Lin et al. 2017; Lu et al. 2019; Chen et al. 2020). Sun et al. (2019) modified the structure of copper-benzene-1,3,5-tricarboxylate (Cu-BTC) MOF by incorporating graphene oxide and reduced graphene oxide (RGO). They investigated the impact of the GO reduction on the selective gas adsorption of the hybrid adsorbent. Dai et al. (2019) reported the adsorption capacity of Cu-BTC/GO composite for toluene as well as the enhanced water stability of the resulting hybrid material. Research conducted by Xia's group (2014) demonstrated that the n-hexane capacity of the MIL-101 composite with GO is significantly higher compared to MIL-101, which is attributed to the higher surface area of the synthesized composite. Additionally, the potential of the MIL-101/GO hybrid structure for the adsorption of heavy metal ions Pb^{2+} from wastewater was established (Lu et al. 2019). In another study by Lim et al. (2020), a copper-metal–organic framework decorated with GO composite was shown as a superior adsorbent for the selective detection of nitrite contamination. He et al. (2021) found that the adsorption capacity of GO/MIL-101(Fe) for the anionic dye methyl orange exceeds that of MIL-101(Fe). The adsorption mechanism of sulfonamide antibiotic onto hybrid materials based on MIL-101(Cr)/GO composite was also investigated (Jia et al. 2019). The MOF-based composite exhibited a removal efficiency of up to 95.5% of polyvinylidene fluoride (PVDF) microplastics (Chen et al. 2020). In a previous study, the removal mechanism of Polyurethane (PU) microplastics using IRMOF-1 metal–organic framework composite based on reduced graphene oxide (IRMOF-1@RGO) was investigated through molecular dynamics (MD) simulations (Shahabi et al. 2024). However, MOF/GO composite research for water treatment is still in its early stages, with few studies on the microscopic performance of MOF/GO composites as adsorbents for the removal of emerging contaminants. In this context, the present work designed a novel multi-scale computational approach to evaluate the removal mechanisms of two types of MPs, including Polyamide 66 (PA66) and PU, by single GO, single Cu-BTC, and Cu-BTC/GO composite. Electronic structure and binding energy analysis, based on density functional theory (DFT) calculations, are conducted to provide detailed insights into the intermolecular interactions between MPs and selected adsorbents. The impact of GO incorporating on the enhancement of the adsorption capacity of pristine MOF during MPs removal has been theoretically investigated in this study.

Methods

Simulation details

Since the objective of this study is to evaluate the removal of MP pollutants from aqueous solutions, we constructed simulation boxes containing eight monomers of each MP and the studied adsorbents with dimensions of $10 \times 10 \times 10 \times 10^{-27}$ m^3 solvated with TIP3P water molecules (Jorgensen et al. 1983). An appropriate number of Na^+/Cl^- ions are then added to ensure the neutrality of the simulation systems.

According to experimental research of Petit and Bandosz (2009), the preferred representation of the MOF/GO hybrid consists of a sandwich of GO shells and MOF core materials. Hence, the designed Cu-BTC/GO composite is constructed by intercalating Cu-BTC into parallel layers of GO, where the oxygen atoms of the basal planes of GOs coordinate with the metal atoms of the MOF component (Petit and Bandosz 2009; Shahabi et al 2024). Representative structures of GO layer, Cu-BTC, and MP monomers are shown in Fig. 1. Figure 2 displays the details of the sandwich structure of the Cu-BTC/GO composite model. Furthermore, the details of the construction of the components for the designed Cu-BTC/GO module are explained in Section S1, Supporting Information. The energy minimization of the initial configuration of each system is conducted using steepest descent method for 50,000 steps. Next, NVT simulations (isothermal-isochoric) are

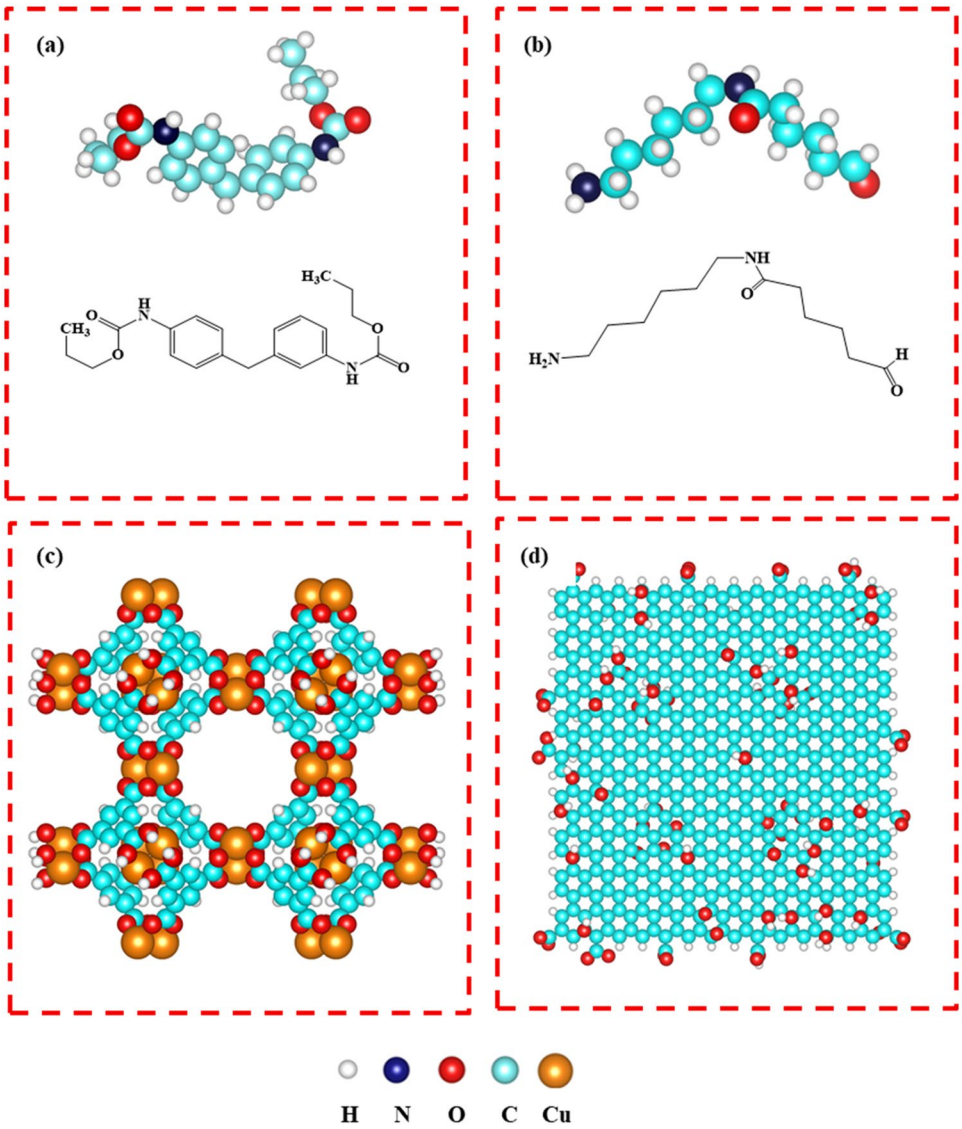

Fig. 1 Schematic illustration of the modeled molecules. Structure of **a** PU monomer, **b** PA66 monomer, **c** Cu-BTC metal–organic framework and **d** GO layer

performed to relax the systems for 1000 ps, followed by NPT simulations (isothermal-isobaric) for 1000 ps. The temperature is maintained using the Nose–Hoover (Evans and Holian 1985) temperature coupling method, and the pressure is controlled using the Parrinello–Rahman algorithm (Parrinello and Rahman 1981). All the production runs are performed under periodic boundary conditions (PBCs) in the NPT ensemble for 90 ns. The long-range electrostatic interactions are treated with the particle mesh Ewald (PME) method (Darden et al. 1993). The entire bond length involving hydrogen atoms is constrained by the LINear Constraint Solver (LINCS) algorithm (Hess et al. 1997). The classical molecular dynamics simulations are conducted in GROMACS (Abraham et al. 2015) software using CHARMM36 force filed with a time step of 1.5 fs.

DFT calculations

A detailed procedure of DFT calculations is provided in Section S2, Supporting Information.

Results

MD simulation

The initial simulation systems including PA66 single, PU single, and binary systems related to the MPs removal efficiency by the designed Cu-BTC/GO composite are shown in Fig. 3. Analysis of the root-mean-square deviation (RMSD) graphs demonstrates that the designed composite is stable

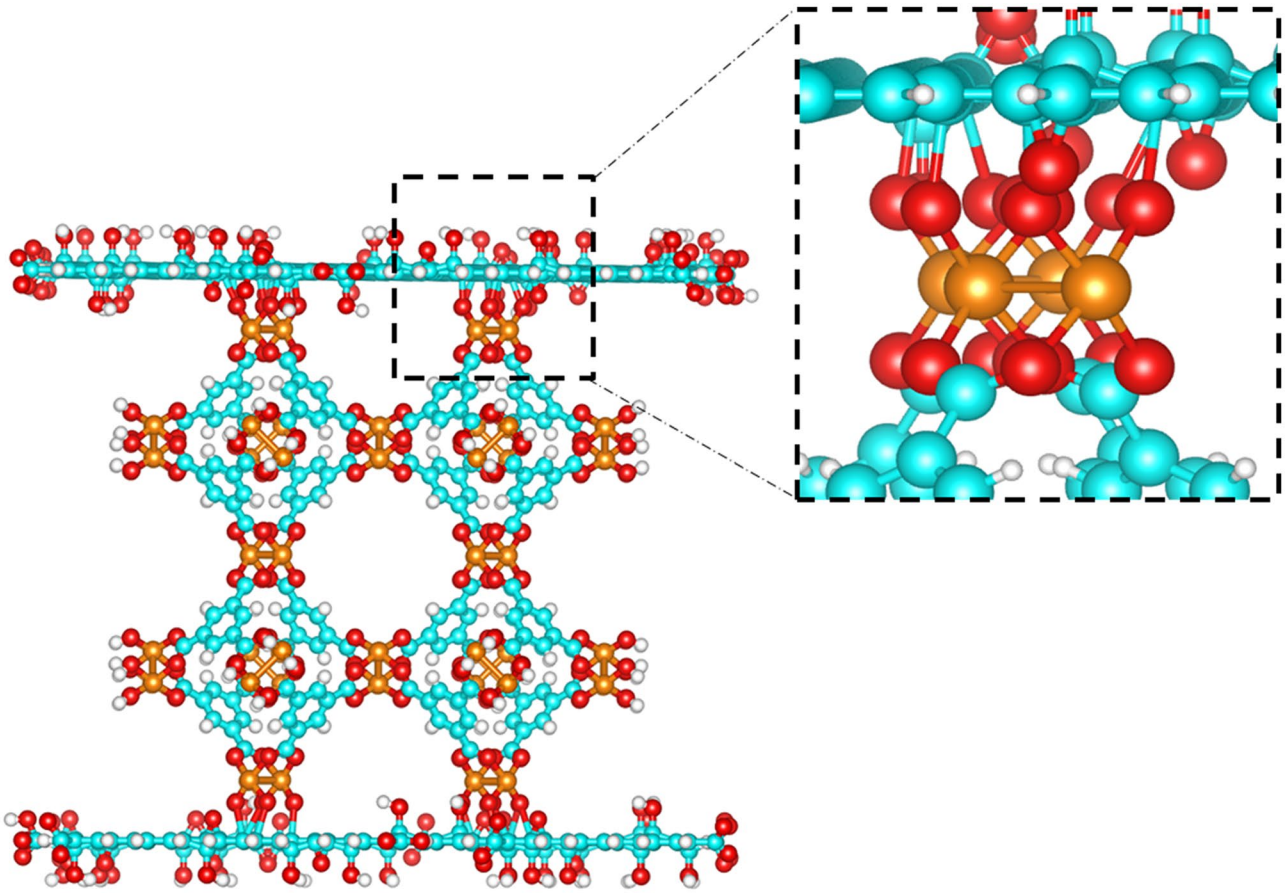

Fig. 2 Model of the designed composite. Details of the sandwich structure of the Cu-BTC/GO composite model

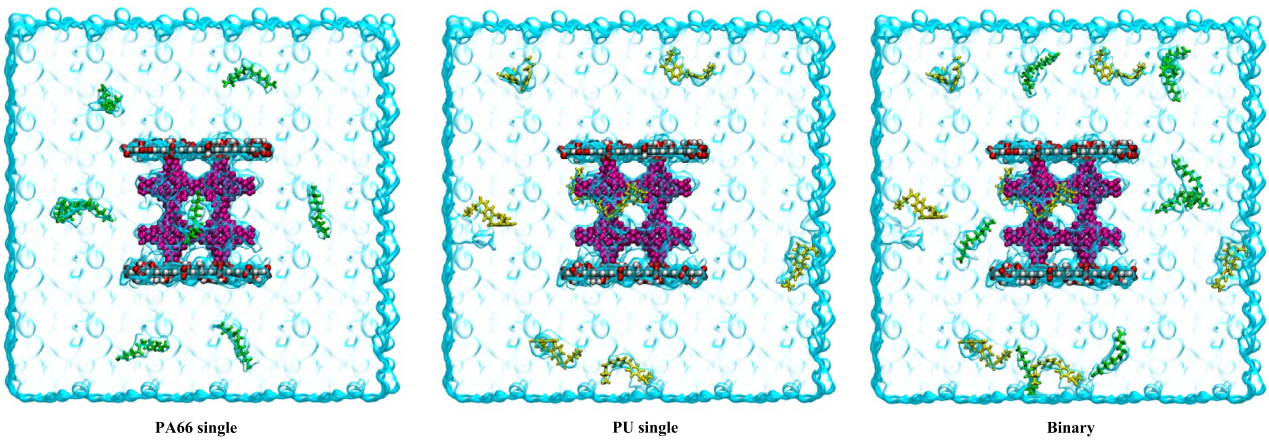

Fig. 3 Initial arrangement of MPs around Cu-BTC/GO composite. The dimensions of the water box in the single-component and binary systems are $10\times10\times10\times10^{-27}$ m^3 and are presented here as a blue surface. Ion molecules are not shown here, but are included in the simulations (color code: PA66: green, and PU: yellow, respectively)

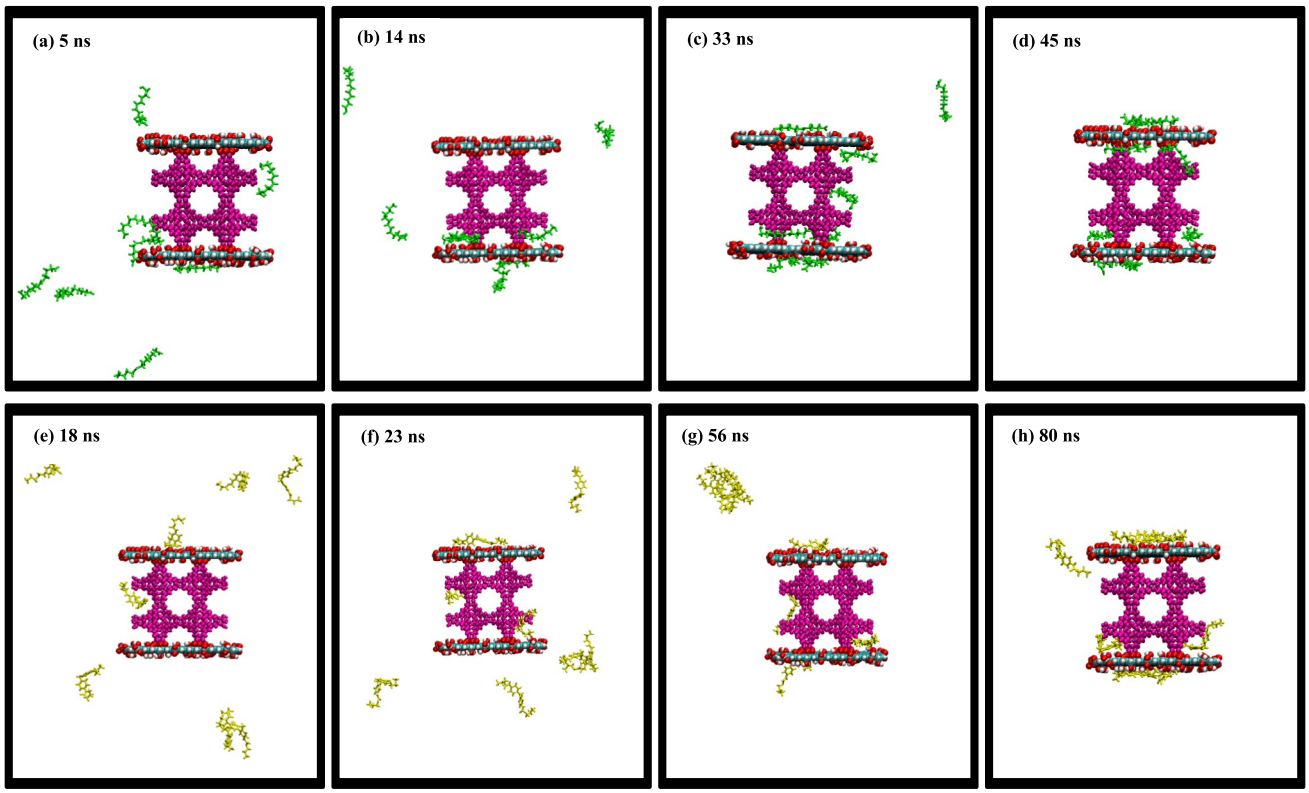

Fig. 4 Investigation of MPs removal process in single-component systems. Representative snapshots of the trajectory for the removal process of PA66 (**a**–**d**) and PU (**e**–**h**) on Cu-BTC/GO adsorbent in the NPT ensemble

and well maintained during 90-ns simulation in the studied systems as shown in Fig. S1, Supporting Information.

The trajectory snapshots of MPs removal by Cu-BTC/GO composite are shown in Fig. 4. Monitoring the simulation trajectory reveals that three PA66 MPs rapidly diffuse from bulk water region to Cu-BTC and GO surface (bottom) in the initial time of simulation (Fig. 4a). As the simulation progresses, two PA66 molecules tend to locate in the interfacial region between Cu-BTC and GO (bottom) as well as in the surface of MOF. It is observed two MPs are trapped in the interfacial region of the Cu-BTC/GO (Fig. 4b). Due to the weak interaction of one MP with MOF, PA66 movement is observed in the vicinity of MOF surface and finally this molecule migrates on the GO surface (bottom). Meanwhile, two PA66 molecules are adsorbed on both sides of GO (top) (Fig. 4c). Within the simulation, it is observed that some MPs are spontaneously adsorbed on the GO surface. Also, PA66 moves toward the GO surface in the interfacial region (Fig. 4d).

It is noted that due to the existence of the active sites in GO to form hydrogen bonds (HBs) with the polar moieties of PA66, the adsorbed molecule does not leave the interfacial region until the end of simulation. As shown in Fig. 4, PU molecules diffuse rapidly from bulk water region toward the composite in the initial time of simulation. It is observed PU molecules adsorb on the surface of MOF and GO (Fig. 4e). Over time of simulation, PU MPs show affinity for the adsorption on GO and the interfacial region of Cu-BTC/GO (bottom) (Fig. 4f). Close inspection of Fig. 4 reveals that a number of MP molecules prefer to form a cluster by overlapping with each other through π–π stacking interactions far away from the adsorbent. This situation is highlighted in Fig. 4g. This dense structure approaches to GO (top) in such a way two MPs adsorb on its surface (Fig. 4h). After that, MPs fluctuate over the composite surface to obtain proper position on GO and Cu-BTC. It is found PA66 molecules are adsorbed on Cu-BTC/GO composite within approximately 45 ns (Fig. 4d). In the case of PU microplastic, this time is about of 80 ns (Fig. 4h).

Different adsorption behavior of MPs in simultaneously removing by Cu-BTC/GO composite is shown in Fig. 5. The intermolecular interaction between PA66 and PU is observed in the initial time of simulation in such a way these small clusters are approached to GO surface (Fig. 5a). Over the time, more affinity of PU toward GO in comparison with PA66 is found (Fig. 5b). As seen, one PA66 molecule tends to adsorb on top of PU microplastic-coated GO surface. Within the simulation, this molecule leaves that situation (Fig. 5c) and loading of PA66 molecule on the exterior surface of Cu-BTC are observed (Fig. 5d).

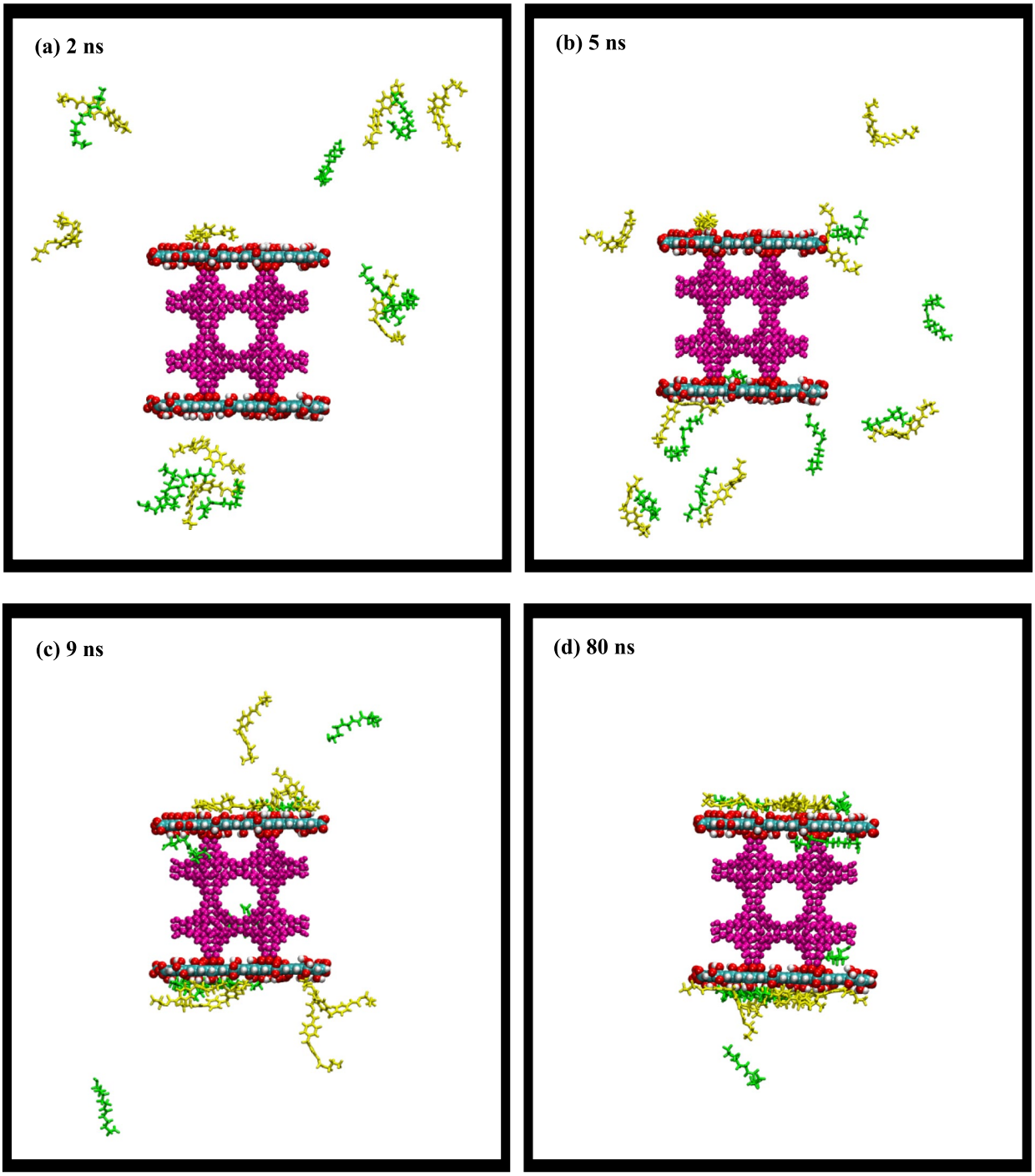

Fig. 5 Investigation of the MPs removal process in a binary system. Representative snapshots for the simultaneous removal process of PA66 (green) and PU (yellow) microplastics in the NPT ensemble

The removal process of two types of MPs by single GO and single Cu-BTC is examined and displayed in Figs. S2 and S3, Supporting Information. The trajectory analysis indicates the adsorption process of PU/PA66 on single GO occurs completely after 25 ns simulation (Fig. S2). In the case of single GO systems, uniform coverage of GO surface by PU/PA66 is observed. MD results demonstrate that single GO exhibits a high MPs loading capacity of 100%. As seen, PA66 molecules are hardly captured by single Cu-BTC, while the uptake capacity of PU is dramatically increased as the simulation progresses (Fig. S3). The self-aggregation of five PU molecules is observed in

the vicinity of Cu-BTC surface, and the diffusion of one microplastic into the large internal cavity of the MOF is found (Fig. S3).

The stability of MPs during the removal process by Cu-BTC/GO composite is also investigated in terms of the gyration radius (R_g), and the results are presented in Fig. S4, Supporting Information. The average solvent-accessible surface area (SASA) for MPs in the simulation systems is also calculated and shown in Fig. S4.

From this figure, a decreasing trend in R_g for PA66 microplastic during 45-ns time of simulation can be attributed to the greater compaction of PA66 on the designed composite, whereas PU still tends to disperse in bulk water rather the interaction with Cu-BTC/GO as observed in the simulation trajectory (Fig. 4). Inspection of Fig. S4a reveals that R_g values of PA66 and PU are stabilized at about 45 ns and 80 ns, indicating single-component systems reach equilibrium thereafter. There is a significant reduction in R_g value of PU from 3.70 nm in PU single system to 2.63 nm in binary system, respectively. This result shows that the interaction of PU with the designed composite is more stable and concentrated in the presence of PA66. As seen, the adsorption capacity of both MPs increases during course of simulation in binary system and reaches equilibrium state in about of 19 ns (Fig. S4a). This result implies the simultaneously removing can facilitate rapid adsorption of PU on the composite surface.

The average values of SASA for PU and PA66 are approximately 50.64 and 40.87 nm^2 in single-component systems, respectively. As observed, the smaller value of SASA for PA66 compared to PU indicates the stronger interaction of this molecule with the designed composite (Fig. S4b). Compared to single-component systems, the reduction SASA for PU is more than that of PA66 in binary system. In other words, the molecular aggregation of PU molecules is reduced in the presence of PA66, which leads to more compact adsorption of PU on the designed composite. This result is in good agreement with the theoretical study of dual removal of PU and dye contaminants (Shahabi et al. 2024). It was demonstrated that competitive adsorption affects the removal process of PU microplastic and its intermolecular interaction with the adsorbent.

The representative snapshots for the final configuration of MPs on Cu-BTC/GO composite as well as on single GO and single Cu-BTC are displayed in Figs. 6 and S5, Supporting Information.

The non-bonding interaction energy including van der Waals (EvdW) and electrostatic (E_{elec}) interactions between MPs and the adsorbents is extracted from the simulation trajectories using "gmx energy" module of GROMACS

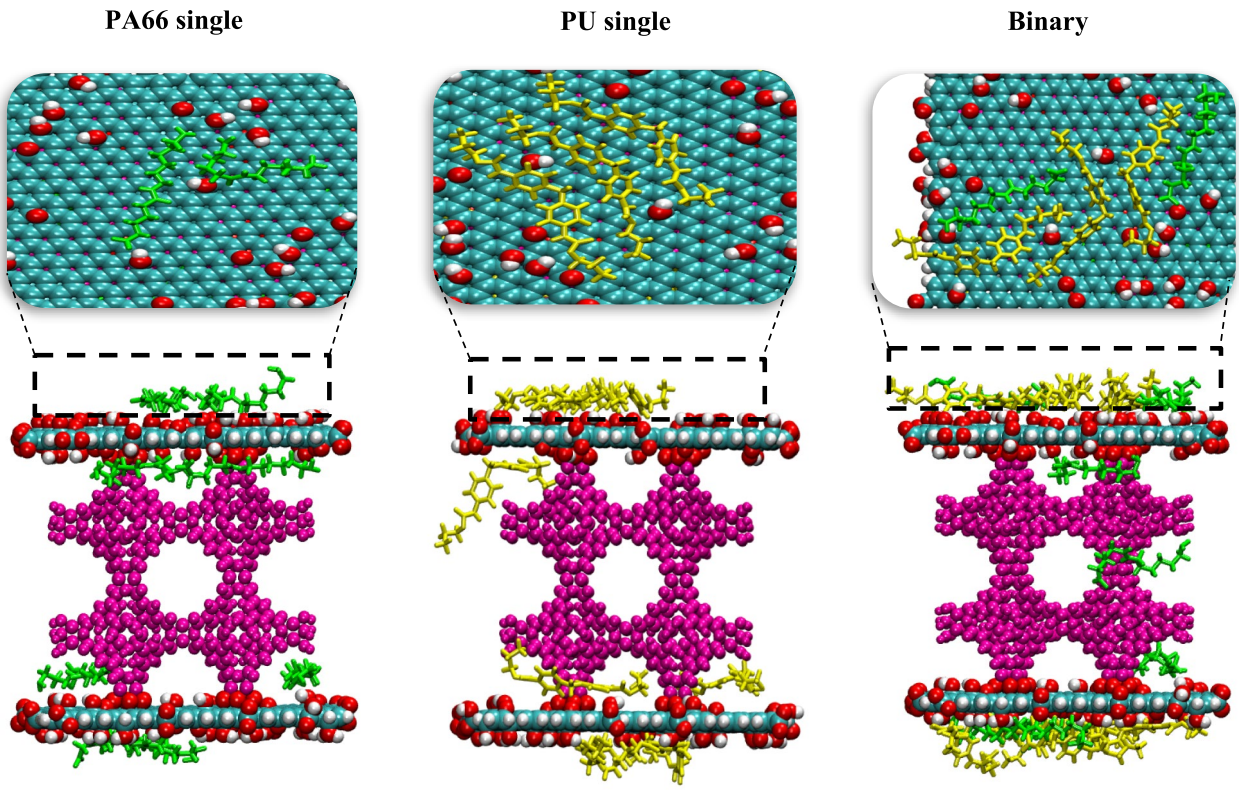

Fig. 6 Final snapshots of MD simulations. Representative snapshots for the final configuration of the MPs adsorbed in single-component and binary systems

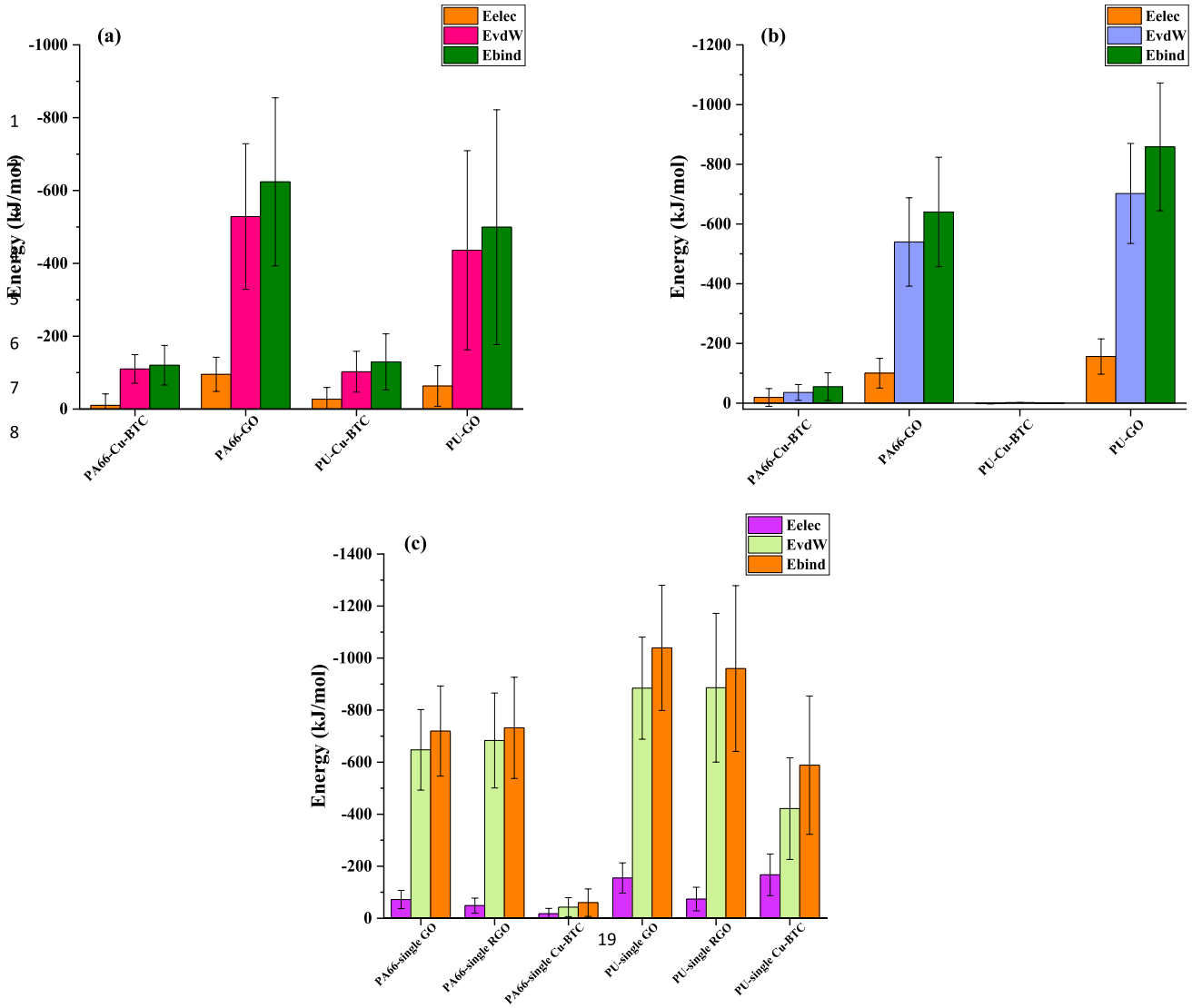

Fig. 7 Analysis of the intermolecular interaction of MPs with the adsorbents. Electrostatic (Eelec), van der Waals (EvdW), and binding (Ebind) energy values between MPs-Cu-BTC and MPs-GO in **a** single-component systems, **b** binary system, and **c** single GO, RGO, and Cu-BTC simulation systems, respectively

software (Abraham et al. 2015). The average values of vdW and electrostatic energies between microplastic-Cu-BTC and microplastic-GO are presented in Fig. 7. In addition, the binding strength (E_{bind}) of MPs, defined as the sum of vdW and electrostatic contributions, is also reported in Fig. 7.

From Fig. 6, a large number of MPs are adsorbed on the GO surface as well as in the interfacial region of Cu-BTC/GO composite in single-component and binary systems. The MD results are consistent with the experimental study of Liu et al. (2013). It is confirmed that the interfacial region created by the connection of GO and Cu-BTC significantly enhances the adsorption performance of the designed composite (Liu et al. 2013; Zhao et al. 2022). As observed, all PU molecules are distributed on the surface of GO components in binary system. Unlike PU, one PA66 molecule captures by Cu-BTC in the vicinity of its large cavity with coexistence of PU (Fig. 6). In the case of single GO, the distribution of PU/PA66 molecules is found on both sides of GO (Fig. S5), whereas the adsorption of PU molecules with less dispersion is observed in a region on the side wall of Cu-BTC. As shown in Fig. S5, PU molecule occupies the large central cavity region of MOF. It is worth noting that the monomer, as the simplest repeating unit of polymer chain, represents the realistic MPs conformation binding during the removal process on the Cu-BTC/GO adsorbent. As observed, the shape and chemical structure of MPs affect their removal efficiency by the designed composite. The aim of the present work is to provide a comprehensive theoretical basis of the

adsorption capacity and removal mechanism of MP on the designed composite. A close inspection of Figs. 6 and S5 shows the adsorption sites are distributed above the benzene rings and oxygen-containing groups on the basal plane of GO components as well as the side walls of the pore in Cu-BTC. Regarding the adsorption sites, π-π stacking, C–H···π interactions and hydrogen bonding promote the adsorption of MPs on the considered adsorbents. It is noted that the aromatic rings of PU adjust their orientation on the benzene rings of the GO surface to form π-π stacking interactions. Furthermore, the C–H···π interactions play the important role in the capture of PA66 by the GO components. In addition, the mechanism of PU pore filling in the single Cu-BTC system is remarkable (Fig. S5). These observations are well accordance with the mechanistic study of MP adsorption on MOF-based composite adsorbent (Shahabi et al. 2024).

The higher uptake capacity of the designed composite for the removal of PA66 is found in single-component systems (Fig. 7; $E_{\text{bind PA66-Cu-BTC/GO}} = -744.22$ kJ/mol and $E_{\text{bind PU-Cu-BTC/GO}} = -629.05$ kJ/mol). MD results show the vdW interaction energy dominates with a small electrostatic contribution between MPs and the components of the composite structure (Fig. 7). This result is in good agreement with the findings of recently reported research, in which hydrophobic interaction is the dominant mechanism in the removal of MPs contaminants (Shang et al. 2022; Bhagwat et al. 2024; Shahabi et al. 2024; Wan et al. 2022). An increase in the adsorption efficiency of Cu-BTC/GO toward PU is observed with the coexistence of PA66, as indicated by the binding energy value of − 858.69 kJ/mol (Fig. 7a, b). Inspection of Fig. 7b reveals PU molecules have no tendency for the interaction with MOF component with neglectable values of the non-bonding interaction energy in binary system. As clearly observed, the interaction between PU and GO is significantly stronger in binary system compared with PU single system. Compared with PU single system, the electrostatic and vdW interaction energy values of PU-GO are changed from − 63.37 kJ/mol to − 156.16 kJ/mol and from − 436.03 kJ/mol to − 702.26 kJ/mol, respectively, with PA66 coexisting. A decreasing trend of the non-bonding interaction energy of PU with GO is associated with more adsorption of PU molecules on six-membered aromatic rings by π–π stacking interactions (Figs. 6 and 7). The interaction strength for the number of MPs adsorbed on single Cu-BTC in the PA66 single Cu-BTC and PU single Cu-BTC systems is about − 59.99 and − 588.55 kJ/mol, respectively (Fig. 7c). From an energetic perspective, the minimum values of the non-bonding interaction energy between PA66 and single Cu-BTC adsorbent can be attributed to the reluctance of MPs to accumulate on the adsorbent, as shown in Fig. S3. Furthermore, the performance of the number of oxygen-containing functional groups in the removal process of MPs by single GO is investigated. Besides GO, the RGO layer which is developed by removing oxygen-containing functional groups from the GO structure is applied, as shown in Fig. S5. It is worth mentioning RGO sheet consists of 10 epoxy, 25 hydroxyl, and 7 carboxyl groups, totaling 49 oxygen atoms with a carbon to oxygen ratio of approximately 10.8. MD simulations reveal that the capacity of RGO to adsorb PU/PA66 is very similar to the oxygen-rich sheet structure for these MPs, but with different strengths (Figs. 7 and S5).

It is found that the addition of oxygen-containing functional groups greatly enhances the electrostatic interaction between MPs and single GO adsorbent.

Figure S6, Supporting Information, shows the variation of atomic contacts between MPs and adsorbents compared with simulation time. Fast diffusion of PA66 toward Cu-BTC/GO composite is accompanied with a sharp increase in the number of atomic contacts from the initial time of simulation (Fig. S6a). The average number of atomic contacts of PA66 with Cu-BTC is fivefold lower than that with GO components in the Cu-BTC/GO composite. A large number of atomic contacts of PU with GO in comparison with MOF confirm the effective loading of MPs on the oxygen-containing groups of the basal plane of GO components in PU single system (Fig. S6b). As shown, PU molecules tend to bind more rapidly and form more intermolecular contacts with GO components in binary system than those with the adsorbent in single-component system. The average number of atomic contacts of PU-GOs is significantly increased from 4200 in the PU single system to 7000 with coexistence of PA66. This result approves PU molecules can be strongly adsorbed on GO surface (Fig. 7). Close inspection of Fig. S6c reveals that there are no intermolecular contacts between PU and Cu-BTC component during 90 ns simulation in binary system. The obtained results are in well agreement with the previously discussed results (Fig. 7). The spontaneous adsorption of MPs on the adsorbents involves the formation of the intermolecular HBs between PU/PA66 and the adsorbent materials. The average number of HBs between microplastic-Cu-BTC and microplastic-GO is reported in Table S1, Supporting Information. Analysis of the average HBs along the simulation trajectory indicates that up to 2.12 and 1.23 HBs are formed between PU-Cu-BTC and PU-GOs in PU single system, respectively. As observed, the enhancement of the number of atomic contacts has positive influence on the increase of HBs number between PA66 and Cu-BTC/GO. In binary system, more intermolecular contacts of PU with GOs are accomplished with more loading on the surface and further more intermolecular HBs numbers (Fig. S6c and Table S1). The average number of HBs between PU-GOs is about of 6.76, while the number of HBs formed between PA66-GOs results to be 3.66 in binary system. According to the number of atomic contacts, the average

HBs formed between PU and Cu-BTC component in the binary system are zero (Table S1).

The probability of finding MPs in terms of the distance relative to the center sites of Cu-BTC/GO components is investigated by radial distribution function (RDF) analysis, and the results are presented in Fig. S7, Supporting Information. Higher strength of RDF profile for both PA66 and PU molecules from GO components in comparison of that during the interaction with Cu-BTC approves more tendency of MPs to accumulate around GO in the single-component systems. However, the peaks exhibit varying magnitudes, indicating the affinity of MPs to GOs is different. The higher peak values of RDF in the removal process of PA66 compared to PU by Cu-BTC/GO demonstrate the stronger attraction of Cu-BTC/GO composite toward PA66 than PU in single-component systems (Fig. S7). Compared to PU single system, the observed peaks between PU-GOs exhibit the prominent function values, which means that a great number of MPs are distributed around GO surface in binary system, as shown in Fig. 6.

DFT analysis

DFT calculations are conducted to determine the energetic and electronic characteristic of MPs removal by GO, Cu-BTC, and GO/Cu-BTC composite in the aqueous phase. The affinity of MP molecules (E_{Ads}) to the considered components is derived from the energy difference between the states of the system, i.e., (Shahabi and Raissi 2020),

$$E_{Ads} = E_{complex} - \left(E_{component} + E_{MP}\right) + E_{BSSE} \quad (1)$$

where $E_{complex}$ is the total energy of the MP molecule adsorbed on the component structures and $E_{component}$ and E_{MP} are the energy of the adsorbents without the MP molecule and the free MP molecule, respectively. E_{BSSE} is the basis set superposition error (BSSE) obtained using the Boys and Bernardi standard counterpoise correction (Boys and Bernardi 1970). The results are given in Table S2, Supporting Information.

Figure S8, Supporting Information, shows the optimized structures of GO, pristine MOF, GO/Cu-BTC composite, and the studied complexes. It is noted that a dicopper tetra-benzenetricarboxylate Cu_2BTC_4 is considered as the molecular model of the Cu-BTC framework (Supronowicz et al. 2013). Comparison of the E_{Ads} energy values shows PU binds strongly to the composite with an energy difference of 66 kJ/mol compared to PA66 ($E_{Ads\ PU@Composite} = -395.09$ kJ/mol), which is better than the values of 0.34 and − 319.61 kJ/mol in the case of pristine MOF and GO, respectively. Higher exothermic interaction energy values are found for PU after adsorption on GO. The interaction energy of GO with PA66 is calculated to be − 307.96 kJ/mol. Inspection of Table S2 reveals that MP molecules have weak intermolecular interactions with pristine MOF. These results clearly demonstrate the involvement of GO in improving the MP removal by the Cu-BTC/GO composite compared to the pristine MOF, as verified by MD simulations. These results are consistent with experimental results (Luo and Wang 2018; Karamipour et al. 2023). It was found that the synergistic effect resulting from the hybridization of MOF with GO plays a remarkable role in improving the removal efficiency of the MOF/GO composite compared to pristine MOF. In other words, the attachment of GO layers to MOFs is a promising method to improve the properties of pristine MOFs as adsorbent materials.

The electron charge density is analyzed by the quantum theory of atoms in molecules (QAIM) method (Shahabi and Raissi 2020) to determine the nature and strength of the adsorption. The values of the electron density (ρ) and its Laplacian ($\nabla^2\rho$) as well as the total electron energy density (H) for the intermolecular interactions are presented in Table S2 and illustrated in Fig. S9, Supporting Information. As seen, the interatomic contacts in all studied complexes have positive values of $\nabla^2\rho$ with $H < 0$, indicating their partial covalent nature. In addition, localized orbital locator (LOL) analysis has been used to validate the nature of the binding as presented in Fig. 8. As evidenced by the low electron density in the space between MPs and the considered adsorbents, both contaminants are involved in the physisorption removal process. Moreover, the changes in the electronic structure and orbital contribution of GO, pristine MOF, and GO/Cu-BTC composite during the interaction with MPs are evaluated by performing total density of states (TDOS) and the projected density of states (PDOS) calculations. The TDOS and PDOS before and after MPs adsorption are displayed in Fig. S10, Supporting Information. Inspection of this figure reveals there is no significant change in the characteristic feature of the PDOS plots of GO, pristine MOF, and the composite compared to the studied complexes. As observed, the PDOS of the adsorbent has a significant contribution from the HOMO (highest occupied molecular orbitals), while the LUMO (lowest occupied molecular orbitals) level comes from the contribution from the MPs orbital.

Potential research outlook of future GO-based metal–organic framework

In the real environment, contaminants exist as a complex mixture rather than as separate entities. The co-occurrence of multiple contaminants may affect the adsorption capacity of each other. The co-exposure of MPs and other pollutants is a source of increasing concern as MPs have been reported to act as carriers of pollutants due to their high sorption capacity. On the other hand, environmental factors

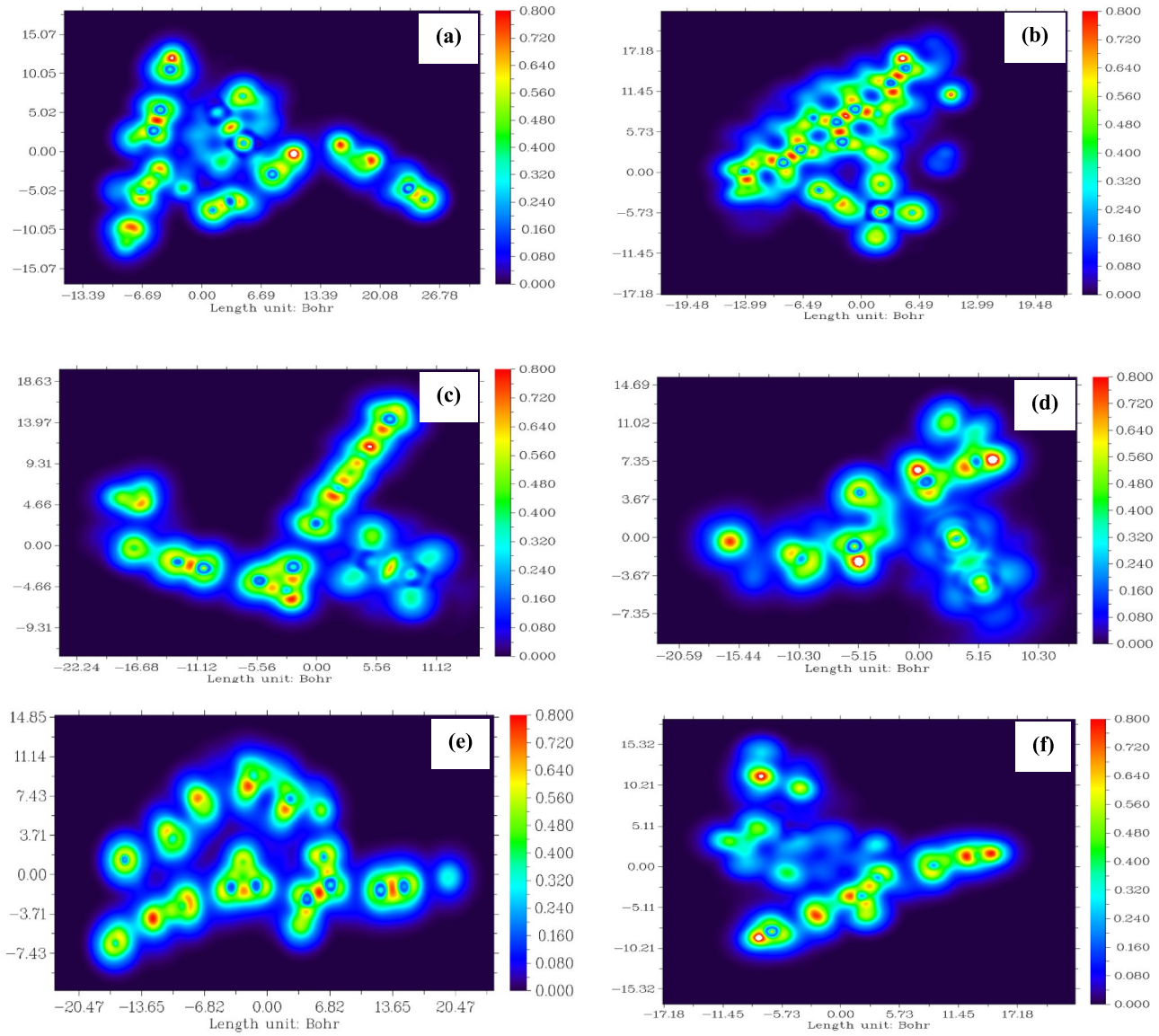

Fig. 8 Illustrations of Localized Orbital Locator (LOL) functions. LOL analysis between MPs and the studied adsorbents shown in **a** PU@Composite, **b** PA66@Composite, **c** PU@MOF, **d** PA66@MOF, **e** PU@GO and **f** PA66@GO, respectively. Covalent regions with high LOL values are shown with red contours, while electron depletion regions (which could indicate non-covalent interaction) are shown with blue contours

have a significant impact on the adsorption of MPs by the designed adsorbent. Therefore, it is necessary to investigate the adsorption performance of the designed Cu-BTC/GO composite under various conditions. However, research on the interaction mechanism of the formed mixture with MPs and other contaminants has been rarely studied due to the complex composition and specific matrix conditions.

To improve the accuracy of the designed model in water treatment, future studies can explore the effect of the composition of the adsorption medium on the adsorption rate of MPs on the designed Cu-BTC/GO adsorbent. The degree of MPs removal efficiency depends on the interaction of contaminants with MPs (Bhagwat et al. 2024), the type of adsorbent (Ali et al. 2023), the composition of aqueous medium, pH, conductivity, temperature, concentration, particle size, shape, and chemical structure of MPs (Magalhães et al. 2020; Ali et al. 2023). Since there is no report of MPs adsorption at the atomic level of the designed Cu-BTC/GO composite, the potential application of Cu-BTC/GO composite in MPs removal requires further research to investigate the effects of coexisting electrolytes, dissolved organic matter, pH, and temperature as well as the degree of polymerization of the polymer chain on the removal process. This future research will provide valuable insights into

Table 1 Summary of characteristics of the reviewed studies on microplastics removal

Materials	MP type	Removal efficiency (%)	References
ZIF-67 MOF	PS	92.1	Wan et al. (2022)
UiO-66-OH@MF-3	PS, PMMA, PVDF	95.5	Chen et al. (2020)
Reduced GO	PS	72	Yuan et al. (2020)
IRMOF-1/RGO	PU	100	Shahabi et al. (2024)
TpPa-OH COF	PE, PET, PA6	100	Shang et al. (2022)
GO	PE	35.66	Uogintė et al. (2023)
GO/PVA	HDPE	95	Dey et al. (2023)
2D MOF@C@FeO	PS	100	Haris et al. (2023)
PSF/MIL-100 (Fe)	PE, PVC	99	Gnanasekaran et al. (2021)
Cu-BTC/GO	PU, PA66	100	This work

PS polystyrene, *PMMA* polymethylmethacrylate, *PVDF* polyvinylidene fluoride, *PE* polyethylene, *PET* polyethylene terephthalate, *PA6* nylon-6, *HDPE* high-density polyethylene, *PVC* polyvinyl chloride

the complex behavior of MPs in Cu-BTC/GO composite systems.

Comparative study

Table 1 summarizes the comparison between various literatures reported for MPs removal. According to the comparison results, there are few reports on MOF-based adsorbents capable of adsorbing MPs. Moreover, MOF-based adsorbents show superior adsorption performance for MPs removal. Hence, the present study highlights the novelty and significant potential of Cu-BTC/GO composite for MPs removal in the field of wastewater treatment.

Conclusion

In summary, MD simulation is applied to explore the capacity of Cu-BTC/GO composite to the individual and simultaneous removal of PA66 and PU molecules from water solution. The combination of GO with MOF enhances the binding energy of MPs toward the designed composite compared to the pristine MOF, as revealed by MD and DFT calculations. The remarkable adsorption performance of the designed composite toward MP pollutants compared to pristine MOF is attributed to HBs, hydrophobic forces, electrostatic attractions, π–π stacking, and intermolecular C–H… π interactions. This study provides a deeper insight into the application of MOF/GO composite for the removal of microplastic at the atomic scale.

Supplementary Information The online version contains supplementary material available at https://doi.org/10.1007/s13201-025-02566-3.

Funding Mahnaz Shahabi was supported by a postdoctoral scholarship from Ferdowsi University of Mashhad (FUM-23954), which is gratefully acknowledged.

Data availability The datasets generated and/or analyzed during the current study are available upon reasonable request from the corresponding author.

Declarations

Conflict of interest The authors declare no competing interests.

References

Abraham MJ et al (2015) GROMACS: high performance molecular simulations through multi-level parallelism from laptops to supercomputers. SoftwareX 1:19–25

Ali I, Asim M, Khan TA (2012) Low cost adsorbents for the removal of organic pollutants from wastewater. J Environ Manag 113:170–183

Ali I, Tan X, Li J et al (2023) Innovations in the development of promising adsorbents for the remediation of microplastics and nanoplastics—a critical review. Water Res 230:119526

Azadpour M et al (2021) Molecular dynamic insight into solubility of H2S in ionic liquids [emim][BF4],[emim][OTf] and [emim][Tf2N]. J Mol Liq 338:117114

Bhagwat KP, Rodrigue D, Romero-Zerón L (2024) Effective removal of microplastic particles from wastewater using hydrophobic biosubstrates. Pollutants 4(2):231–250

Bhoria N et al (2020) Functionalization effects on HKUST-1 and HKUST-1/graphene oxide hybrid adsorbents for hydrogen sulfide removal. J Hazard Mater 394:122565

Botas JA et al (2011) Effect of Zn/Co ratio in MOF-74 type materials containing exposed metal sites on their hydrogen adsorption behaviour and on their band gap energy. Int J Hydrog Energy 36(17):10834–10844

Boys SF, Bernardi FJMP (1970) The calculation of small molecular interactions by the differences of separate total energies. Some procedures with reduced errors. Mol Phys 19(4):553–566

Chen G (2004) Electrochemical technologies in wastewater treatment. Sep Purif Technol 38:11–41

Chen YJ et al (2020) Metal–organic framework-based foams for efficient microplastics removal. J Mater Chem A 8(29):14644–14652

Cole M et al (2011) Microplastics as contaminants in the marine environment: a review. Mar Pollut Bull 62(12):2588–2597

Dahanayaka M et al (2020) Atomistic simulation study of GO/HKUST-1 MOF membranes for seawater desalination via pervaporation. Appl Surf Sci 503:144198

Dai Y, Li M, Liu F et al (2019) Graphene oxide wrapped copper-benzene-1, 3, 5-tricarboxylate metal organic framework as efficient absorbent for gaseous toluene under ambient conditions. Environ Sci Pollut Res Int 26:2477–2491

Darden T, York D, Pedersen L (1993) The effect of long-range electrostatic interactions in simulations of macromolecular crystals–a comparison of the Ewald and truncated list methods. J Chem Phys 99:10089

DeCoste JB et al (2013) The effect of water adsorption on the structure of the carboxylate containing metal–organic frameworks Cu-BTC, Mg-MOF-74, and UiO-66. J Mater Chem A 1(38):11922–11932

Dey TK, Jamal M, Uddin ME (2023) Fabrication and performance analysis of graphene oxide-based composite membrane to separate microplastics from synthetic wastewater. J Water Process Eng 52:103554

Domán A et al (2020) Graphene oxide protected copper benzene-1, 3, 5-tricarboxylate for clean energy gas adsorption. Nanomater 10(6):1182

Evans DJ, Holian BL (1985) The nose–hoover thermostat. J Chem Phys 83(8):4069–4074

Gnanasekaran G, Arthanareeswaran G, Mok YS (2021) A high-flux metal-organic framework membrane (PSF/MIL-100 (Fe)) for the removal of microplastics adsorbing dye contaminants from textile wastewater. Sep Purif Technol 277:119655

Górka J et al (2010) Mesoporous metal organic framework–boehmite and silica composites. Chem Commun 46(36):6798–6800

Guo XX et al (2020) Catalytic degradation of anthraquinones-containing H_2O_2 production effluent over layered Co-Cu hydroxides: defects facilitating hydroxyl radicals generation. Appl Catal B Environ 260:118157

Hamzeh Ali H et al (2020) Synthesis of GO-Cu-BTC graphene oxide at the Green and in situ under solvent-free conditions by the mechanochemical methods and evaluation of kinetic and isotherm properties of cadmium removal. J Appl Res 14(2):127–135

Haris M et al (2023) Self-assembly of C@ FeO nanopillars on 2D-MOF for simultaneous removal of microplastic and dissolved contaminants from water. Chem Eng J 455:140390

He W et al (2021) Preparation of a GO/MIL-101 (Fe) composite for the removal of methyl orange from aqueous solution. ACS Omega 6(7):4597–4608

Hess B et al (1997) Lincs: a linear constraint solver for molecular simulations. J Comput Chem 18:1463–1472

Hosseini M et al (2024) Investigations of nickel silicate for degradation of water-soluble organic pollutants. Int J Hydrog Energy 61:307–315

Jia X et al (2019) Adsorption behavior and mechanism of sulfonamide antibiotics in aqueous solution on a novel MIL-101 (Cr)@ GO composite. J Chem Eng Data 64(3):1265–1274

Jorgensen WL et al (1983) Comparison of simple potential functions for simulating liquid water. J Chem Phys 79(2):926–935

Kang J et al (2019) Degradation of cosmetic microplastics via functionalized carbon nanosprings. Matter 1(3):745–758

Karami M et al (2022) Green fabrication of graphene quantum dots from cotton with $CaSiO_3$ nanostructure and enhanced photocatalytic performance for water treatment. Int J Hydrog Energy 47(11):7228–7241

Karamipour M, Fathi S, Safari M (2023) Removal of phenol from aqueous solution using MOF/GO: synthesis, characteristic, adsorption performance and mechanism. Int J Environ Anal Chem 103(16):3853–3864

Levasseur B, Petit C, Bandosz TJ (2010) Reactive adsorption of NO_2 on copper-based metal−organic framework and graphite oxide/metal−organic framework composites. ACS Appl Mater Inter 2:3606–3613

Lim HN et al (2020) Ultrasonic assisted synthesis of size-controlled Cu-metal–organic framework decorated graphene oxide composite: sustainable electrocatalyst for the trace-level determination of nitrite in environmental water samples. ACS Omega 5(24):14242–14253

Lin LC, Paik D, Kim J (2017) Understanding gas adsorption in MOF-5/graphene oxide composite materials. Phys Chem Chem Phys 19(18):11639–11644

Liu S et al (2013) Nanosized Cu-MOFs induced by graphene oxide and enhanced gas storage capacity. Energy Environ Sci 6(3):818–823

Liu W et al (2019) Selective adsorption and removal of drug contaminants by using an extremely stable Cu (II)-based 3D metal-organic framework. Chemosphere 215:524–531

Lu M et al (2019) Highly efficient removal of Pb^{2+} by a sandwich structure of metal–organic framework/GO composite with enhanced stability. New J Chem 43(2):1032–1037

Luo S, Wang J (2018) MOF/graphene oxide composite as an efficient adsorbent for the removal of organic dyes from aqueous solution. Environ Sci Pollut Res 25(6):5521–5528

Magalhães S et al (2020) Microplastics in ecosystems: from current trends to bio-based removal strategies. Molecules 25:3954

Millward AR, Yaghi OM (2005) Metal−organic frameworks with exceptionally high capacity for storage of carbon dioxide at room temperature. J Am Chem Soc 127(51):17998–17999

Mu Y et al (2009) Decolorization of azo dyes in bioelectrochemical systems. Environ Sci Technol 43(13):5137–5143

Mulfort KL, Hupp JT (2007) Chemical reduction of metal−organic framework materials as a method to enhance gas uptake and binding. J Am Chem Soc 129(31):9604–9605

Neghlani PK, Rafzadeh M, Taromi FA (2011) Preparation of aminatedpolyacrylonitrile nanofber membranes for the adsorption of metal ions: comparison with microfbers. J Hazard Mater 186(1):182–189

O'Neill LD, Zhang H, Bradshaw D (2010) Macro-/microporous MOF composite beads. J Mater Chem 20(27):5720–5726

Othmani A et al (2021) Biochar and activated carbon derivatives of lignocellulosic fibers towards adsorptive removal of pollutants from aqueous systems: critical study and future insight. Sep Purif Technol 274:119062

Parrinello M, Rahman A (1981) Polymorphic transitions in single crystals: a new molecular dynamics method. J Appl Phys 52:7182–7190

Petit C, Bandosz TJ (2009) MOF–graphite oxide composites: combining the uniqueness of graphene layers and metal–organic frameworks. Adv Mater 21:4753–4757

Petit C, Bandosz TJ (2011) Synthesis, characterization, and ammonia adsorption properties of mesoporous metal-organic framework (MIL (Fe))-graphite oxide composites: exploring the limits of materials fabrication. Adv Funct Mater 21:2108–2117

Petit C, Mendoza B, Bandosz TJ (2010) Reactive adsorption of ammonia on Cu-based MOF/graphene composites. Langmuir 26(19):15302–15309

Pourmand S et al (2025) Assessment of dynamic removal mechanism of non-steroidal anti-inflammatory biomolecules in the aqueous environments by a novel covalent organic framework. J Mol Graph 137:109006

Shahabi M, Raissi H (2020) Two dimensional porous frameworks of graphyne family as therapeutic delivery vehicles for Idarubicin biomolecule in silico: density functional theory and molecular dynamics simulation. J Mol Liq 319:114334

Shahabi M, Ahmadpour A, Raissi H (2024) Assessment of water purification by IRMOF-1 based on rGO as a new nanoengineered adsorbent: Insights from adsorption mechanism. J Mol Liq 400:124485

Shang S et al (2022) Studying the adsorption mechanisms of nanoplastics on covalent organic frameworks via molecular dynamics simulations. J Hazard Mater 421:126796

Stock N, Biswas S (2012) Synthesis of metal-organic frameworks (MOFs): routes to various MOF topologies, morphologies, and composites. Chem Rev 112(2):933–969

Sui X et al (2019) The roles of metal-organic frameworks in modulating water permeability of graphene oxide-based carbon membranes. Carbon 148:277–289

Sun Y et al (2019) Graphene modified Cu-BTC with high stability in water and controllable selective adsorption of various gases. J Alloys Compd 808:151721

Supronowicz B, Mavrandonakis A, Heine T (2013) Interaction of small gases with the unsaturated metal centers of the HKUST-1 metal organic framework. J Phys Chem C 117(28):14570–14578

Tabatabaeinejad SM et al (2021) Dy2Cu2O5 nanostructures: sonochemical fabrication, characterization, and investigation of photocatalytic ability for elimination of organic contaminants. J Mol Liq 344:117883

Uogintė I et al (2023) Degradation and optimization of microplastic in aqueous solutions with graphene oxide-based nanomaterials. Int J Environ Sci Technol 20(9):9693–9706

Varghese AM et al (2021) Enhancing effect of UV activation of graphene oxide on carbon capture performance of metal-organic framework/graphene oxide hybrid adsorbents. Chem Eng J 420:129677

Varjani S et al (2020) Microbial degradation of dyes: An overview. Bioresour Technol 314:123728

Wan H et al (2022) Removal of polystyrene microplastics from aqueous solution using the metal–organic framework material of ZIF-67. Toxics 10(2):70

Wu J, Eiteman MA, Law SE (1998) Evaluation of membrane filtration and ozonation processes for treatment of reactive-dye wastewater. J Environ Eng ASCE 124(3):272–277

Xia Q et al (2014) Synthesis and adsorption performance of MIL-101 (Cr)/graphite oxide composites with high capacities of n-hexane. Chem Eng J 239:226–232

Xiang Z et al (2011) Metal–organic frameworks with incorporated carbon nanotubes: improving carbon dioxide and methane storage capacities by lithium doping. Angew Chem Int Ed Engl 50(2):491–494

Yousefzadeh F, Ghanbari M, Salavati-Niasari M (2023) Sonochemical synthesis and characterization of Sm2CuO4 nanostructures and their application as visible-light photocatalyst for degradation of water-soluble organic pollutants. Chemosphere 338:139564

Yuan F et al (2020) Study on the adsorption of polystyrene microplastics by three-dimensional reduced graphene oxide. Water Sci Technol 81(10):2163–2175

Zhao Y et al (2013) Aminated graphite oxides and their composites with copper-based metal–organic framework: in search for efficient media for CO_2 sequestration. Rsc Adv 3(25):9932–9941

Zhao H et al (2022) Insights into the performance of hybrid graphene oxide/MOFs for CO_2 capture at process conditions by molecular simulations. J Chem Eng 449:137884

Zhou M, Särkkä H, Sillanpää MA (2021) comparative experimental study on methyl orange degradation by electrochemical oxidation on BDD and MMO electrodes. Sep Purif Technol 78(3):290–297